Title: Synthesis and characterization of magnetic chitosan microspheres as low-density and low-biotoxicity adsorbents for lake restoration

Authors: A. Funes[a,b*], J. de Vicente[c] and I. de Vicente[a,b]

Affiliations: (a) Departamento de Ecología, Facultad de Ciencias, Universidad de Granada, 18071 Spain

(b) Instituto del Agua, Universidad de Granada, 18071 Spain

(c) Departamento de Física Aplicada, Facultad de Ciencias, Universidad de Granada, 18071 Spain

Full address for correspondence:

[*] Corresponding author.

Departamento de Ecología, Facultad de Ciencias, Universidad de Granada, 18071 Spain

Phone: (+34) 958 248323; Fax: (+34) 958 243093 ; email: afunes@ugr.es

Keywords: magnetite, magnetic chitosan, emulsion, phosphorus, eutrophication

Abstract

We propose a novel magnetic adsorbent for optimal Phosphorus (P) removal from the upper sediment layers. For this aim, magnetic chitosan microparticles were prepared using a reverse-phase suspension cross-linking technique. The resulting particles and suspensions were characterized using scanning electron microscopy, X-ray powder diffraction, Fourier transform infrared spectroscopy, magnetometry, thermogravimetric analysis, electrophoretic mobility and turbidity measurements. The hybrids are multi-core particles consisting of well dispersed magnetite nanoparticles (approx. 10 % w/w) homogeneously distributed within the biopolymer matrix. These microparticles can be easily separated from the water column and sediment using magnetic field gradients. Their P adsorption capacity is evaluated in batch conditions resulting in a maximum P adsorption capacity of M_L = 4.84 mg g^{-1} at pH = 7. We demonstrate that these particles are excellent candidates to remove P from water column and also P mobile from the upper sediment layers due to two main reasons: they sediment slower and present lower potential toxicity (due to a their larger size) than conventional iron/iron oxide microparticles previously proposed for lake restoration.

1. Introduction

Enrichment of phosphorus (P) is considered the main cause of eutrophication of inland waters (Carpenter, 2005). In situations in which P release from sediment (internal P load) impedes lake recovery once external P load has been reduced, in-lake addition of P-binding adsorbents appears as an advisable alternative for lake management (Cooke et al., 2005; Søndergaard et al., 2003). Z2G1 or Aqual-P®, Phoslock®, calcium, iron (Fe) or alum salts have been demonstrated to increase sediment P-sorption capacity (Cooke et al., 2005; Dittrich et al., 2011; Gibbs et al., 2011; Robb et al., 2003; Søndergaard et al., 2003). Although some of these techniques could represent a long-lasting sink for P, changes in physicochemical conditions or resuspension events can lead to undesirable P release to water column along with toxic substances stemming from the adsorbents composition (Egemose et al., 2009; Zamparas and Zacharias, 2014).

In the last decades, magnetic nano- and microparticles have attracted special attention to adsorb contaminants from waters and soils due to their easy separation and recovery from the medium for further reuse. This obviously leads to cost savings and to the reduction of the contact time with biota (Crane and Scott, 2012; Gómez-Pastora et al., 2014; Huber, 2005; Lu et al., 2007; Tang and Lo, 2013). With this in mind, more recently, these magnetic particles have been successfully used for P removal in the context of lake restoration and improvement of water quality (Choi et al., 2016; Daou et al., 2007; de Bashan and Bashan, 2004; de Vicente et al., 2010; Funes et al., 2016, 2014; Lai et al., 2016; Long et al., 2011; Shaikh and Dixit, 1992).

Apart from high P adsorption capacity and reusability, magnetic particles must meet other stringent requirements for lake restoration applications. Particle size has very important implications not only in adsorption capacity but also in biological toxicity.

Small (nano) particles are preferred to enhance adsorption capacity (because of their large surface area) (Yavuz et al., 2006). However, there are evidences of toxicological effects on aquatic organisms (Oberdörster, 2004); because cladocerans such as *Daphnia sp*. filter large volumes of water, considerable amounts of nanoparticles can be ingested by them, having negative consequences in their physiology and also in upper levels of the food chain (Lovern and Klaper, 2006, Zhu et al., 2010). Unfortunately, nanoparticles can also negatively affect aquatic biota by adsorption on their carapaces and filtrations apparatus (Baumann et al., 2014). Finally, Fe dissolution is another indirect effect of using Fe based nanoparticles which can led to phytotoxicity (Keller et al., 2012).

Of outstanding importance in this work is particle density. Actually, particle density is a key factor driving adsorbent distribution through the sediment profile and determines its availability for P adsorption. It is worth to stress here that sedimentary P mobile, which is the target P pool, mostly concentrates within the first 10 cm of sediment and decreases rapidly with depth (Reitzel et al., 2005). From this perspective, very large density particles are not desirable because they sink deeper in sediment being not available for P adsorption. Moreover, sinking of magnetic particles into deeper layers may contribute to intense sediment resuspension when removing the magnetic particles with the magnet causing undesirable effects (Søndergaard et al., 1992). In addition, large density particles may sink into the deepest sediment layers where magnetophoretic forces exerted by the magnets could not be large enough to overcome opposing surface (cohesive) forces within the sediment making the recovery process inefficient (Yavuz et al., 2006). Thus, a balance between high P removal efficiency (high affinity and large surface area), low bio-toxicity (biocompatible components and large particle size to difficult the ingestion by biota) and low density (to remain in the first 10 cm of sediment) must be pursued (Philippova et al., 2011; Reddy and Lee, 2013).

In this work, we fabricate hybrid magnetic particles (magnetic chitosan microspheres, MCMs) that accomplish the three requirements discussed in paragraph above. We follow a novel approach that consists in the encapsulation of magnetic multicores within a biopolymer spherical matrix that prevents Fe dissolution, is non-toxic and less dense (than traditional magnetic adsorbents), but still exhibiting a large adsorption capacity for lake restoration applications. Furthermore, by using a chitosan matrix we introduce versatile adsorption properties (apart from the traditional specific adsorption mechanism between P and Fe oxides) that can be controlled through the cross-linker concentration due to the presence of amine and hydroxyl groups and therefore pH dependent electrostatic interactions.

2. Materials and Methods

All reagents were of analytical grade and used without further purification. $FeCl_3 \cdot 6H_2O$, ethylene glycol (EG) and sodium acetate (NaAc) were supplied from VWR (AnalaR-Normapur). Trisodium citrate (Na_3Cit) was obtained from Carlo Erba. Chitosan (low molecular weight; 75-80 % deacetylated), glutaraldehyde (8%), mineral oil, Span 80 and petroleum ether were acquired from Sigma Aldrich. Acetic acid (5%) and acetone were obtained from Panreac. Finally, carbonyl Fe microparticles were obtained from BASF (grade HQ, average diameter = 800 nm, Germany).

2.1 Synthesis of magnetite (Fe_3O_4) nanoparticles

There are several routes for the synthesis of Fe_3O_4 depending on the particle size to be obtained. For instance, Fe_3O_4 nanoparticles of typical sizes in the range ~ 10 nm can be prepared by the Massart's method (Massart, 1981). In this case, Fe^{+2} and Fe^{+3} are coprecipitated in an alkaline solution. Another option to obtain Fe_3O_4 particles in the

micronsized range, ~ 1000 nm, is to follow Sugimoto and Matijevic (1980). In this case, Fe^{+2} oxidation is slowed down by a nitrate salt allowing the particles to grow larger. In this particular work, we are interested in particles having an intermediate particle size (~ 100 nm): large enough to respond to magnetophoretic forces and small enough for a large surface activity and hence adsorption capacity.

We used a solvothermal method following the recommendations by Liu et al. (2009a) with slight modifications. Briefly, 3.38 g of $FeCl_3 \cdot 6H_2O$ (0.25 mol L^{-1}) and 0.5 g of Na_3Cit (34 mmol L^{-1}) were dissolved in 50 mL of ethylene glycol by using a centrifugal mixer (3 min at 1000 rpm). NaAc (3 g) was then added and the suspension was mixed again (15 min at 1000 rpm). Next, the mixture was sealed in a Teflon-lined stainless-steel autoclave (125 mL capacity) and heated at 215 ºC for 10 h. The obtained magnetic nanoparticles were washed several times with ethanol and dried at 50 ºC for 4 hours.

2.2 Preparation of magnetic chitosan microspheres (MCMs)

MCMs where fabricated by a reverse-phase suspension cross-linking technique following Jiang et al. (2005) with slight modifications. First, previously synthesized Fe_3O_4 powder (0.082 g) was dispersed via ultrasonication in a solution of chitosan (0.25 g) in 5% acetic acid (10 mL) for 10 min. The Fe_3O_4:chitosan ratio (by weight) was 1:3. Next, 10 mL of this suspension were added drop-wise to a mixture of mineral oil (37.5 mL) and Span 80 (2.5 g) as a surfactant. During all the process, the formed emulsion was stirred with a mechanical stirrer at 2500 rpm for 30 min. Then, 5 mL of glutaraldehyde were added dropwise and the dispersion was stirred for another 1 h at 40 ºC to promote the cross-linking. Finally, the magnetic microspheres were separated from the oil phase by applying a magnet for 30 min and washed several times with petroleum ether and acetone. MCMs were then dried at 50 ºC for 4 h and stored until use. Chitosan micro-

spheres (CMs) were prepared following the same procedure as MCMs without addition of Fe_3O_4. CMs were separated from oil phase by centrifugation at 3000 rpm for 5 min, washed and stored as in MCMs procedure.

2.3 Characterization of the hybrid particles

Size and surface morphology of Fe_3O_4, MCMs and CMs particles were elucidated with high-resolution field-emission scanning electron microscopy (FIB-FESEM, AURIGA, Carl Zeiss SMT Inc.). Environmental scanning electron microscopy (ESEM, FEI Quanta 400) was used to determine internal distribution of Fe_3O_4 particles within MCMs. Samples were embedded within an Epofix resin and cross-sectioned. Crystal structure of Fe_3O_4 and MCMs was analyzed with a Bruker D8 Advance X-Ray difractometer (XRD) with scattering angle (2θ) of 0-90º using Cu-Kα as incident radiation (λ = 0.1540 Å) at 40 kV. Fourier transform infrared spectroscopy (FT-IR) was recorded between 4000-400 cm^{-1} on a JASCO 6200 spectrophotometer in attenuated total reflection (ATR) mode to observe interactions between functional groups of the different synthesized systems. Samples were prepared with KBr disks. Thermal stability of the different composites was analyzed by a thermogravimetric analyzer (METTLER TOLEDO mod.DCS1). Samples were heated from 37 to 950 ºC with a heating rate of 10 ºC min^{-1} in N_2 atmosphere. The magnetization measurements of the composites were performed with a SQUID magnetometer (MPMS XL, Quantum Desing) at room temperature. The external field was swept from -4000 to 4000 kA m^{-1}. Electrophoretic mobility of the composites was determined using a Zetasizer Nano Z (Malvern instruments, UK) at 25 ºC. To minimize sedimentation of magnetic particles under gravity, prior to the test, the samples were sonicated for 5 min. Samples for measuring electrophoretic mobility were prepared as follows: a suspension of Fe_3O_4 (0.1 g L^{-1}) or MCMs (0.72 gL^{-1}) or CMs

(0.62 g L^{-1}) with 3 mM $NaHCO_3$ was agitated for 24 h in a horizontal shaker (150 rpm) at different pH values. Afterwards, pH was readjusted and the suspensions were made up to 25 mL of volume. Turbidity measurements were performed using a Turbiscan MA 2000 (Formulaction, France) in order to compare sedimentation rates of MCMs and carbonyl Fe microparticles used by de Vicente et al. (2010). Briefly, dispersions were placed in a cylindrical plastic cell which was scanned from the bottom to the top with an incident near infrared light source (λ_{air} = 850 nm; Wulff-Pérez et al., 2009). Measurements reported here only consider transmission data -as a function of sample height and time-. Samples were prepared by mixing a suspension of carbonyl Fe microparticles (0.1 g L^{-1}) or MCMs (0.72 g L^{-1}) with 3 mM $NaHCO_3$ under agitation for 24 h at pH 7 in a final volume of 25 mL.

2.4 Batch adsorption experiments

Fe_3O_4, MCMs and CMs stock suspensions were prepared by mixing either 100 mg or 720 mg or 620 mg, respectively, with 100 mL of distilled water in a polyethylene container. Suspensions were sonicated for 5 min prior to their use for adsorption experiments to ensure homogeneity of the dispersion. As 2.5 mL of the stock solution (1 g Fe_3O_4 L^{-1}; 7.2 g MCMs L^{-1}; 6.2 g CMs L^{-1}) were added to a final volume of 25 mL, the final concentration for each suspension was 0.1 g Fe_3O_4 L^{-1}, 0.72 g MCMs L^{-1} and 0.62 g CMs L^{-1}.

To investigate the effect of pH on P removal efficiency by MCMs, 2.5 mL of a MCMs stock suspension (7.2 g L^{-1}) were mixed with 20 mL of 3 mM $NaHCO_3$ (acting as a buffer) and shaked for 24 h in a horizontal shaker (150 rpm). Then, 2 mL of a 0.125 mM P stock solution were added to each tube and pH was adjusted to 7, 8 and 9. Suspensions were shaked (150 rpm) for 24 h. After this time, pH was readjusted and the

volume was made up to 25 mL with 3 mM $NaHCO_3$. Initial P concentration accounted for 0.01 mM P. A magnetic separation gradient (PASCO scientific; EM-8641) was applied for 5 min and the supernatant was filtered to measure P by spectrophotometric procedure according to Murphy and Riley (1962).

Maximum P adsorption capacity was tested by adding 2.5 mL of the corresponding stock suspension to 20 mL 3 mM $NaHCO_3$ in 25 mL centrifuge tubes. Final adsorbent concentrations of Fe_3O_4 and CMs isotherms were fixed according to Fe_3O_4 and chitosan content in MCMs as obtained from magnetometry tests. Suspensions were shaked (150 rpm) for 24 h and then, 2 mL of KH_2PO_4 solutions with P concentrations ranging from 0.125 to 2 mM P were added. The pH value was adjusted to 7 and suspensions were shaked again (150 rpm) for 24 h. Afterwards, pH was readjusted and the volume was made up to 25 mL with 3 mM $NaHCO_3$. The magnetic separation gradient was applied for 5 min and P determination was carried out as previously mentioned. The equilibrium adsorption capacity of P, q, was calculated as follows:

$$q = \frac{C_0 - C_e}{M_a} V \quad [1]$$

where C_0 and C_e are the initial and equilibrium P concentration (mg L^{-1}), respectively, M_a is the mass of adsorbent in grams and V is the total volume of the suspension (L).

3. Results and discussion

3.1 Characterization of composites

Fig. S1 (supplemental material) shows a typical SEM image of the Fe_3O_4 particles. As observed, they are quasi-spherical in shape and uniform in size with a mean diameter of about 280 nm. A detailed description of their morphological characteristics is provided

198 in Table S1 (supplemental material). Higher magnification images indicate that Fe_3O_4
199 consisted of clusters of small nanocrystals (Fig. S1 inset). CMs were also visualized
200 under the microscope. As demonstrated in Fig. S2 (supplemental material), they were
201 spherical in shape but significantly larger, and more polydisperse, than Fe_3O_4 nanoparti-
202 cles (~3200 nm average number diameter with a polydispersity index of 1.7, Table S1).
203 Fig. 1a reveals that MCMs were also polydisperse and spherical in shape with larger
204 diameter than CMs (average number diameter ~4800 nm). More details on the morpho-
205 logical characteristics of the particles can be found in Table S1. In contrast to CMs,
206 MCMs showed a grainy surface (Fig. 1a inset) whereas CMs surface was smooth (Fig.
207 S2 inset). The cross-sectioned MCMs depicted in Fig. 1b revealed a homogeneous dis-
208 tribution of Fe_3O_4 nanoparticles within the chitosan microspheres indicating that the
209 embedding process resulted in little Fe_3O_4 aggregation.

210 Fig. S3 (supplemental material) shows the XRD patterns of Fe_3O_4 and MCMs particles.
211 Six diffraction peaks at 2θ = 30.18°, 35.5°, 43.16°, 53.37°, 56.86° and 62.71° were
212 clearly identified in both composites. These peaks fit to Fe_3O_4 according to the Joint
213 Committee on Powder Diffraction Standards (JPCS) database but it is difficult to differ-
214 entiate between Fe_3O_4 and γ-Fe_2O_3 since both have similar spinel structures and there-
215 fore similar XRD patterns (Zhou et al., 2002). The broad peak at 2θ = 20.53° is ascribed
216 to the presence of chitosan (Kyzas and Deliyanni, 2013). Results corroborate that Fe_3O_4
217 is embedded within the chitosan matrix and the lower intensity found in MCMs com-
218 pared to bare Fe_3O_4 comes from the amorphous chitosan structure.

219 FT-IR spectra of the synthesized Fe_3O_4, MCMs and CMs particles are shown in Fig. S4
220 (supplemental material). For comparison, this figure also includes the spectra corre-
221 sponding to chitosan powder. The sharp peak at 587 cm^{-1} is assigned to vibrations of

Fe-O bonds in Fe_3O_4 (Tian et al., 2011). This characteristic peak is also present in MCMs but shifts to 621 cm^{-1}. The absorptions at 1607 and 1385 cm^{-1} in Fe_3O_4 are attributed to stretching vibrations of C=O bonds indicating the presence of carboxyl groups coming from a thin layer of Na_3Cit stabilizer on the surface of Fe_3O_4 particles in agreement with Liu et al. (2009a) . For chitosan powder the N-H band vibration is found at around 1639 cm^{-1} (Agnihotri and Aminabhavi, 2004). In MCMs and CMs a new peak appears at around 1563 cm^{-1} which is ascribed to ethylenic bond (C=N) indicating the reaction of carboxyl groups of glutaraldehyde and amine groups of chitosan to form the *Schiff base* (Kumar et al., 2009; Li et al., 2013; Monteiro and Airoldi, 1999). The absorption band at 1720 cm^{-1} indicates the presence of free aldehydic group in CMs whereas no evidence was found for MCMs (Monier et al., 2012) . A peak around 2923 cm^{-1} is related to streching vibration of C-H bonds (Chen and Park, 2003; Zhang et al., 2011). The broad peak at 3437 cm^{-1} assigned to O-H bond stretching or N-H bond stretching increased in intensity in the case of MCMs possibly indicating high proportion of unreacted free amine and/or hydroxyl groups compared to CMs (Iyengar et al., 2014; Monier et al., 2012).

Magnetization curves of the Fe_3O_4 and MCMs particles at 293 K are represented in Fig. 2. Fe_3O_4 and MCMs behave as soft magnetic materials with no coercivity and remanence pointing out that the single-domain magnetic nanoparticles persisted in MCMs (Zhang et al., 2010). The saturation magnetization (*Ms*) of the synthesized Fe_3O_4 (64 emu g^{-1}) is well below the theoretical value for bulk Fe_3O_4 (84 emu g^{-1}) (Philippova et al., 2011) but close to that obtained by Liu et al. (2009a) (73 emu g^{-1}). This is explained by a reduction in crystallinity due to the presence of Na_3Cit during synthesis process and surface organic coating (Liu et al., 2009a). Obviously, embedding magnetic particles within the chitosan matrix results in reduction of *Ms* value (Gómez-Pastora et al.,

247 2014; Liu et al., 2009b). Using the reference value for the synthesized Fe_3O_4, the mag-
248 netic content of the hybrid particles is approx. 14% w/w. This magnetite loading is
249 clearly lower than 33 % (i.e. Fe_3O_4:chitosan ratio of 1:3) hence suggesting that some
250 magnetic nanoparticles are not encapsulated within the chitosan microspheres during the
251 emulsification process. As will be seen later, MCMs retained a magnetic character that
252 is enough to ensure separation from the medium when applying an external magnetic
253 field (see below).

254 TGA measurements for the different particles are summarized in Fig. S5 (supplemental
255 material). Fe_3O_4 showed an important weight loss (16 %) in the range of 37-678 ºC
256 which is slightly higher than that reported by Liu et al. (2009a). A weight loss of about
257 3% occurred from 37 ºC to 180 ºC. This corresponds to the evaporation of water mole-
258 cules adsorbed on the surface of Fe_3O_4 (Cai and Wan, 2007) . The most significant
259 weight loss (13%) occurred in the interval 180-678 ºC. This is attributed to the removal
260 of the Na_3Cit organic compound used during Fe_3O_4 synthesis (Liu et al., 2009a). Fi-
261 nally, a slight weight gain of approximately 2 % was observed in the range 678-950 ºC,
262 attributed to the oxidation of Fe_3O_4 to γ-Fe_2O_3 (Tian et al., 2011) . MCMs showed a
263 11% of weight loss below 180 ºC due to the removal of adsorbed water. However, the
264 most significant degradation was at 180-550 ºC corresponding to breakage of chitosan
265 chains (Kalkan et al., 2012) and this continues until 950 ºC. CMs started to degrade at
266 lower temperature than pure chitosan indicating than cross-linking reduces thermal sta-
267 bility (Li et al., 2013; Neto et al., 2005). Also, CMs showed less thermal stability than
268 MCMs due to the absence of Fe_3O_4. Chitosan powder showed an overall 76% of weight
269 loss. A slight weight loss of 9 % is observed below 100 ºC and ascribed to the release of
270 adsorbed water molecules (Kumar and Koh, 2012). However, it is mostly degraded be-
271 tween 300-500 ºC (Kalkan et al., 2012). The magnetic content of the hybrid particles as

estimated from TGA measurements is approx. 9 % w/w. This result is in reasonably good agreement with magnetometry measurements reported in the paragraph above.

3.2 Turbidity measurements: sedimentation

The penetration of the particles within the sediment layer depends on the sedimentation rate. Generally speaking, the sedimentation rate V of a colloidal suspension is governed by the density mismatch between the particles ρ_p and the carrier fluid ρ_c, particle diameter d, gravity constant g, continuous phase dynamic viscosity ν and particle volume fraction ϕ (Mills and Snabre, 1994) :

$$V = \frac{|\rho_p - \rho_c| g d^2}{18 \nu \rho_c} \frac{1-\phi}{1+\frac{4.6\phi}{1-\phi^3}} \quad [2]$$

In the case of MCMs particles, the $|\rho_p - \rho_c|$ term clearly approaches to zero (if compared to classical Fe particles) and hence the sedimentation rate is expected to be reduced if the other parameters remain fixed in Equation [2]. However, the diameter of the MCMs particles is approximately 5 times larger than carbonyl Fe (see Table S1) and this contributes, as well, to increase the sedimentation rate.

As a result, turbidity measurements were also performed to interrogate the sedimentation characteristics of MCMs suspensions and ascertain whether they sediment slower than carbonyl Fe. For completeness carbonyl Fe suspensions were also measured at the same particle concentration (0.72 g L^{-1}). A sedimentation process was clearly observed in both systems, demonstrated by an increase in the transmission profiles (clarification) at the top of the sample with a concomitant decrease of transmission at the bottom of the sample (Fig. S6a and S6b, supplemental material). Clarification in the whole height of the tube also evidenced aggregation of the dispersed particles in both suspensions,

294 although it was more intense for carbonyl Fe microparticles. Fig. 3 represents the time
295 evolution of the sedimentation front (H/H_0) for the two suspensions. In the case of car-
296 bonyl Fe particles, the sedimentation front experienced a marked decrease over time
297 reaching a constant value of 20% after 5 min whereas MCMs showed a much lower
298 sedimentation over time reaching the constant value of 20% after 30 min.

299 These results demonstrate that the sedimentation rate of MCMs is slower than carbonyl
300 Fe microparticles despite of their higher particle diameter (average diameter: carbonyl
301 Fe microparticles = 800 nm; MCMs = 4800 nm). This is explained by the lower density
302 of MCMs compared to carbonyl Fe microparticles.

303 *3.3 P removal efficiency by MCMs: effect of pH*

304 In general, pH has an important influence on the nature of the adsorbent and adsorbate
305 (Gómez-Pastora et al., 2014) . Therefore, the P removal efficiency by MCMs is ex-
306 pected to be influenced by the pH. Results obtained for MCMs are summarized in Fig.
307 4. This figure shows that the highest P removal efficiency (75% P removal) corresponds
308 to pH = 7. A significant reduction in P uptake (ANOVA; $F_{2,6}$ = 441.2, p value < 0.001)
309 was found with increasing pH value to pH = 8 (58% P removal) and pH = 9 (24 % P
310 removal). Different P adsorption efficiencies are reported in the literature for neutral pH
311 conditions. A lower P reduction (23%), but the same decreasing tendency with pH, was
312 found by Yao et al. (2014) when using ammonium-functionalized magnetic chitosan.
313 Filipkowska et al. (2014) found a 40 % of P reduction when using glutaraldehyde cross-
314 linked chitosan. Dixon (1984) reported a high P removal (85 %) by Fe_3O_4 that de-
315 creased with raising pH. Contrary to the results for MCMs, P adsorption efficiency by
316 bare carbonyl Fe microparticles is not pH dependent in the pH range (6-10) leading to a
317 high P reduction (80% P removal) whatever the pH (de Vicente et al., 2010). These re-

sults were explained by de Vicente et al. (2010) because of specific adsorption onto the particles. It is worthy to highlight that initial P concentrations used by some of the mentioned authors were much higher than those used in this work.

Our results point out that pH dependency of the P adsorption onto MCMs is due to the surface charge of the adsorbent and speciation of the adsorbate. MCMs are positively charged in the pH range of 7-9 but the magnitude of charge decreases with pH (see electrophoretic mobility data in Fig. 4). Electrophoretic mobility measurements seem to be related to the P removal efficiency of the particles. Huang et al. (2010) also reported positively charged magnetic chitosan nanopaticles in pure water. At lower pH, amine groups of chitosan are more easily protonated than at higher pH values (Crini and Badot, 2008). At low pHs, P exists as both anions, dyhydrogen phosphate ($H_2PO_4^-$) and hydrogen phosphate (HPO_4^{2-}) (Eliaz and Sridh, 2008) thus leading to the conclusion that P adsorption onto MCMs is dominated by electrostatic interactions.

3.4 P maximum adsorption capacity

The adsorption data of the different adsorbents used in this study were fitted to Langmuir isotherm (Foo and Hameed, 2010):

$$q = \frac{K_L M_L C_e}{1+K_L C_e} \quad [3]$$

where K_L is an adsorption constant related to energy of adsorption (L g^{-1}) and M_L is an empirical saturation constant that represents the maximum adsorption capacity (mg g^{-1}) (Foo and Hameed, 2010; Wong et al., 2004).

In the three cases, the Langmuir model showed a satisfactory fit to the experimental data. In the case of MCMs and CMs (Fig. 5), at low phosphate concentrations, the ad-

sorption increased when increasing concentration but tended to reach a constant value at higher phosphate concentrations in accordance to the model (Biswas et al., 2008) . Although the same adsorption mechanism could be applied to Fe_3O_4, the saturation value was reached very quickly compared to MCMs and CMs (Fig. 5). Table 1 shows the best fitting parameters for Fe_3O_4, MCMs and CMs, and the corresponding correlation coefficients. Note that for comparative purposes, in these experiments, the magnetite concentration was the same (constant) in Fe_3O_4 and MCMs suspensions. Also, the chitosan concentration in CMs and MCMs suspensions was kept the same. The highest maximum P adsorption capacity (M_L) was reported by MCMs (4.84 mg g^{-1}) followed by CMs (2.41 mg g^{-1}) and Fe_3O_4 (2.27 mg g^{-1}). Table 1 also summarizes maximum P adsorption capacities of different adsorbents of interest found in the literature. P adsorption capacity values of Phoslock® (Haghseresht, 2005; Zamparas et al., 2012), alum (de Vicente et al., 2008) or some clays such as Zenit/Fe (Zamparas et al., 2012) and clinoptilolite (Sakadevan and Bavor, 1998) are closer to values obtained for MCMs. On the contrary, synthetic zeolite HUD (Onyango et al., 2007) and CFH-12 (Lyngsie et al., 2014) present much higher P sorption capacities compared to MCMs. Isotherm data pointed out a P removal efficiency by MCMs higher than 45 % for concentrations ranging from 10 to 160 µmol P L^{-1} when using a concentration of 0.72 g MCMs L^{-1}. Then, it can be stated that MCMs would be potentially able to remove 60 % of P from water column of hypertrophic water bodies whose average water column TP have been determined to be higher than 100 µg L^{-1} (3.23 µmol P L^{-1}) (Nürnberg, 1996).

Differences in P adsorption capacity of Fe_3O_4, MCMs and CMs can be explained by the different surface characteristics of the systems. The low P adsorption capacity found for Fe_3O_4 is in the range of that found by Daou et al. (2007) (although at a different pH value; pH = 3) who reported a maximum P adsorption capacity of 5.2 mg P g^{-1} (Table 1)

when using a positively charged Fe_3O_4 with higher surface area (40 nm average particle size). However, a much higher P adsorption capacity is also reported in the literature for the same pH conditions to our study. de Vicente et al. (2010) found that negatively charged Fe_3O_4 (90 nm) was able to adsorb a maximum of 27.15 mg P g^{-1} (Table 1). At pH = 7, our Fe_3O_4 exhibits a negative surface charge (electrophoretic mobility -2.7 ± 0.45 µm cm V^{-1} s^{-1}) which suggests that P adsorption mechanism is driven by specific interactions (and not by electrostatic interactions). The comparatively low P adsorption capacity found in our Fe_3O_4 is explained by the organic layer (supported by TGA and FT-IR analysis) covering Fe_3O_4 surface that may difficult P adsorption onto hydroxyl functional groups present on its surface (Antelo et al., 2005; Sun et al., 1998).

CMs adsorption capacity reported in this work is low compared to other studies employing cross-linked chitosan composites with the same pH conditions as the cases of Filipkowska et al. (2014) and Sowmya and Meenakshi (2014) who reported a P maximum adsorption capacity of 58.5 mg $g^{-1}$and 108.2 mg g^{-1}, respectively (Table 1). Synthesized CMs showed a slight negative surface charge as indicated by electrophoretic mobility (-0.84 ± 0.65 µm cm V^{-1} s^{-1}) similarly to other cross-linked chitosan composites (Yao et al., 2014). Indeed, the point of zero charge (pzc) for most chitosan particles has been previously reported to range between 6.2 and 6.7 (Chatterjee et al., 2005; Elwakeel, 2009). P adsorption onto CMs is thought to be due to physical adsorption or intraparticle diffusion through the chains network of the particle (Crini and Badot, 2008).

It is noteworthy that MCMs are positively charged despite of the fact that Fe_3O_4 and CMs are negatively charged at pH = 7. This is expected because the embedded magnetite grains interfere in the cross-linking process. The reason is that chitosan surface charge is determined by protonation/deprotonation of its surface functional groups

(amine and hydroxyl groups) depending on pH (Pillai et al., 2009; Reddy and Lee, 2013). During the synthesis process in acidic media, aldehyde groups of glutaraldehyde mainly react with protonated amine and hydroxyl groups (Crini and Badot, 2008). As suggested in previous works, a higher extent of cross-linking reduces particle size and surface zeta potential due to condensation of polymer chains and reduction of positively charged free amino groups, respectively (Crini and Badot, 2008; He et al., 1999; Rodrigues et al., 2012). In our case, the larger particle size of MCMs (compared to CMs) suggests a lower degree of cross-linking that is expected and attributed to the physical interference of magnetite in the Schiff´s base reaction giving a net positive charge to the hybrid particles.

Reuse of MCMs is essential for their practical use and cost effectiveness. In this context, a conventional protocol that works well in the case of iron oxides consists in washing the particles with a concentrated NaOH solution. With this in mind, after a typical adsorption experiment, the MCMs particles were washed twice with 1M NaOH and 3 times with 3 mM $NaHCO_3$ using magnetic separation. This particular protocol although successful for magnetite and carbonyl Fe particles (de Vicente et al., 2010) failed in the case of MCMs (the P adsorption capacity of reused particles was very low). Degradation of the adsorbent may be another important issue for practical applications. However, chitosan solubilisation is not likely to occur in natural environments because strong acidic conditions are required (Crini and Badot, 2008). Nevertheless, the cross-linking level in MCMs may definitely have an effect and its impact in the resulting chemical stability and mechanical resistance of the microparticles are open issues for future work.

4. Conclusions

We propose a novel magnetic adsorbent for P removal from the upper sediment layers. It consists on very low density hybrid multigrain microparticles prepared by a reverse-phase suspension cross-linking technique. The microparticles are constituted by well dispersed magnetite nanocores within a spherical chitosan microparticle (approx. 10 % w/w) that is biocompatible and non toxic. These particles do exhibit a sufficient P adsorption capacity (M_L = 4.84 mg g^{-1}) to be used in eutrophic systems at conventional pH levels. The mechanism behind the adsorption is dual: electrostatic for the case of chitosan matrix and surface specific for the case of magnetite grains. This provides versatile adsorption properties toward cation species as well. Because of their large size and magnetite loading, these hybrid microparticles can be easily separated using magnetophoresis.

Apart from their versatile adsorption properties, the major advantage of these particles is that, once settled from the water column, they have the ability to remain in the upper layers of the sediment where the target sedimentary P pool in eutrophic lakes (P mobile) concentrates. This is due to their much lower particle density compared to other magnetic adsorbents previously proposed for lake restoration. Another interesting aspect of the synthesized microparticles is the low toxicity for aquatic biota due to their high particle size. Further investigation about MCMs reutilization is still needed in order to make these particles cost-effective as P adsorbents.

Acknowledgments

The authors would like to thank F. Galisteo-González for providing the Bool2k software used for the generation of particle-size distributions from SEM micrographs and F. Vereda for his help in the Chemistry Laboratory. This work was supported by Junta de Andalucía projects of excellence P10-RNM-6630 and P11-FQM-7074 (Spain);

437 MINECO CTM 2013-46951-R, MAT 2013-44429-R and PCIN 2015-051, MAT 2016-
438 78778-R projects (Spain); and by the European Regional Development Fund (ERDF).

References

Agnihotri, S.A., Aminabhavi, T.M., 2004. Controlled release of clozapine through chitosan microparticles prepared by a novel method. J. Control. Release 96, 245–259. doi:10.1016/j.jconrel.2004.01.025.

Antelo, J., Avena, M., Fiol, S., López, R., Arce, F., 2005. Effects of pH and ionic strength on the adsorption of phosphate and arsenate at the goethite-water interface. J. Colloid Interface Sci. 285, 476–486. doi:10.1016/j.jcis.2004.12.032.

Baumann, J., Köser, J., Arndt, D., Filser, J., 2014. The coating makes the difference: Acute effects of iron oxide nanoparticles on Daphnia magna. Sci. Total Environ. 484, 176–184. doi:10.1016/j.scitotenv.2014.03.023.

Biswas, B.K., Inoue, K., Ghimire, K.N., Harada, H., Ohto, K., Kawakita, H., 2008. Removal and recovery of phosphorus from water by means of adsorption onto orange waste gel loaded with zirconium. Bioresour. Technol. 99, 8685–8690. doi:10.1016/j.biortech.2008.04.015.

Cai, W., Wan, J., 2007. Facile synthesis of superparamagnetic magnetite nanoparticles in liquid polyols. J. Colloid Interface Sci. 305, 366–370. doi:10.1016/j.jcis.2006.10.023

Carpenter, S.R., 2005. Eutrophication of aquatic ecosystems: bistability and soil phosphorus. Proc. Natl. Acad. Sci. U. S. A. 102, 10002–10005. doi:10.1073/pnas.0503959102.

Chatterjee, S., Chatterjee, S., Chatterjee, B.P., Das, A.R., Guha, A.K., 2005. Adsorption of a model anionic dye, eosin Y, from aqueous solution by chitosan hydrobeads.

J. Colloid Interface Sci. 288, 30–35. doi:10.1016/j.jcis.2005.02.055.

Chen, X.G., Park, H.J., 2003. Chemical characteristics of O-carboxymethyl chitosans related to the preparation conditions. Carbohydr. Polym. 53, 355–359. doi:10.1016/S0144-8617(03)00051-1.

Choi, J., Chung, J., Lee, W., Kim, J.O., 2016. Phosphorous adsorption on synthesized magnetite in wastewater. J. Ind. Eng. Chem. 34, 198–203. doi:10.1016/j.jiec.2015.11.008.

Cooke, G.D., Welch, E.B., Peterson, S.A., Nichols, S.A., 2005. Restoration and management of lakes and reservoirs, third edition, Taylor and Francis Group, Boca Raton, Florida.

Crane, R.A., Scott, T.B., 2012. Nanoscale zero-valent iron: Future prospects for an emerging water treatment technology. J. Hazard. Mater. 211-212, 112–125. doi:10.1016/j.jhazmat.2011.11.073.

Crini, G., Badot, P.M., 2008. Application of chitosan, a natural aminopolysaccharide, for dye removal from aqueous solutions by adsorption processes using batch studies: A review of recent literature. Prog. Polym. Sci. 33, 399–447. doi:10.1016/j.progpolymsci.2007.11.001.

Daou, T.J., Begin-Colin, S., Grenche, J.M., Thomas, F., Derory, A., Bernhardt, P., Legar, P., Pourroy, G., 2007. Phosphate adsorption properties of magnetite-based nanoparticles. Chem. Mater. 19, 4494–4505. doi:10.1021/cm071046v.

de Vicente, I., Huang, P., Andersen, F., Jensen, H.S., 2008. Phosphate adsorption by fresh and aged aluminum hydroxide. Consequences for lake restoration.

Environ. Sci. Technol. 42, 6650–6655. doi:10.1021/es800503s.

de Vicente, I., Merino-Martos, A., Cruz-Pizarro, L., de Vicente, J., 2010. On the use of magnetic nano and microparticles for lake restoration. J. Hazard. Mater. 181, 375–381. doi:10.1016/j.jhazmat.2010.05.020.

de-Bashan, L.E., Bashan, Y., 2004. Recent advances in removing phosphorus from wastewater and its future use as fertilizer (1997-2003). Water Res. 38, 4222–4246. doi:10.1016/j.watres.2004.07.014.

Dittrich, M., Gabriel, O., Rutzen, C., Koschel, R., 2011. Lake restoration by hypolimnetic $Ca(OH)_2$ treatment: Impact on phosphorus sedimentation and release from sediment. Sci. Total Environ. 409, 1504–1515. doi:10.1016/j.scitotenv.2011.01.006.

Dixon, D.R., 1984. Colour and turbidity removal with reusable magnetite particles-VII. A colloid chemistry study of the effect of inorganic ions on the efficiency of clarification. Water Res. 18, 529–534. doi:10.1016/0043-1354(84)90199-4.

Egemose, S., Wauer, G., Kleeberg, A., 2009. Resuspension behaviour of aluminium treated lake sediments: effects of ageing and pH. Hydrobiologia 2, 1–15. doi:10.1007/s10750-009-9949-8.

Eliaz, N., Sridh, T.M., 2008. Electrocrystallization of hydroxyapatite and its dependence on solution conditions. Cryst. Growth Des. 8, 3965–3977. doi:10.1021/cg800016h.

Elwakeel, K.Z., 2009. Removal of Reactive Black 5 from aqueous solutions using magnetic chitosan resins. J. Hazard. Mater. 167, 383–392.

doi:10.1016/j.jhazmat.2009.01.051.

Filipkowska, U., Jóźwiak, T., Szymczyk, P., 2014. Application of cross-linked chitosan for phosphate removal from aqueous solutions. Prog. Chem. Appl. Chitin Its Deriv. 19, 5–14. doi:10.15259/PCACD.19.01.

Foo, K.Y., Hameed, B.H., 2010. Insights into the modeling of adsorption isotherm systems. Chem. Eng. J. 156, 2–10. doi:10.1016/j.cej.2009.09.013.

Funes, A., de Vicente, J., Cruz-Pizarro, L., Álvarez-Manzaneda, I., de Vicente, I., 2016. Magnetic microparticles as a new tool for lake restoration: A microcosm experiment for evaluating the impact on phosphorus fluxes and sedimentary phosphorus pools. Water Res. 89, 366–374. doi:10.1016/j.watres.2015.11.067.

Funes, A., de Vicente, J., Cruz-Pizarro, L., de Vicente, I., 2014. The influence of pH on manganese removal by magnetic microparticles in solution. Water Res. 53, 110–122. doi:10.1016/j.watres.2014.01.029.

Gibbs, M.M., Hickey, C.W., Özkundakci, D., 2011. Sustainability assessment and comparison of efficacy of four P-inactivation agents for managing internal phosphorus loads in lakes: Sediment incubations. Hydrobiologia 658, 253–275. doi:10.1007/s10750-010-0477-3.

Gómez-Pastora, J., Bringas, E., Ortiz, I., 2014. Recent progress and future challenges on the use of high performance magnetic nano-adsorbents in environmental applications. Chem. Eng. J. 256, 187–204. doi:10.1016/j.cej.2014.06.119.

Haghseresht, F., 2005. A revolution in phosphorus removal, Phoslock Water Solution Ltd. http://www.phoslock.com.au p. 21.

He, P., Davis, S.S., Illum, L., 1999. Chitosan microspheres prepared by spray drying. Int. J. Pharm. 187, 53–65. doi: 10.1016/S0378-5173(99)00125-8.

Huang, H.Y., Shieh, Y.T., Shih, C.M., Twu, Y.K., 2010. Magnetic chitosan/iron (II, III) oxide nanoparticles prepared by spray-drying. Carbohydr. Polym. 81, 906–910. doi:10.1016/j.carbpol.2010.04.003.

Huber, D.L., 2005. Synthesis, properties, and applications of iron nanoparticles. Small 1, 482–501. doi:10.1002/smll.200500006.

Iyengar, S.J., Joy, M., Ghosh, C.K., Dey, S., Kotnala, R.K., Ghosh, S., 2014. Magnetic, X-ray and Mössbauer studies on magnetite/maghemite core–shell nanostructures fabricated through an aqueous route. RSC Adv. 4, 64919–64929. doi:10.1039/C4RA11283K.

Jiang, D.S., Long, S.Y., Huang, J., Xiao, H.Y., Zhou, J.Y., 2005. Immobilization of Pycnoporus sanguineus laccase on magnetic chitosan microspheres. Biochem. Eng. J. 25, 15–23. doi:10.1016/j.bej.2005.03.007.

Kalkan, N.A., Aksoy, S., Aksoy, E.A., Hasirci, N., 2012. Adsorption of reactive yellow 145 onto chitosan coated magnetite nanoparticles. J. Appl. Polym. Sci. 124, 576-584. doi: 10.1002/app.34986.

Keller, A.A., Garner, K., Miller, R.J., Lenihan, H.S., 2012. Toxicity of nano-zero valent iron to freshwater and marine organisms. PLoS One 7, 1–10. doi:10.1371/journal.pone.0043983.

Kumar, S., Dutta, J., Dutta, P.K., 2009. Preparation and characterization of N-heterocyclic chitosan derivative based gels for biomedical applications. Int. J.

Biol. Macromol. 45, 330–337. doi:10.1016/j.ijbiomac.2009.08.002.

Kumar, S., Koh, J., 2012. Physiochemical, optical and biological activity of chitosan-chromone derivative for biomedical applications. Int. J. Mol. Sci. 13, 6103–6116. doi:10.3390/ijms13056102.

Kyzas, G.Z., Deliyanni, E.A., 2013. Mercury(II) removal with modified magnetic chitosan adsorbents. Molecules 18, 6193–6214. doi:10.3390/molecules18066193.

Lai, L., Xie, Q., Chi, L., Gu, W., Wu, D., 2016. Adsorption of phosphate from water by easily separable Fe_3O_4@SiO_2 core/shell magnetic nanoparticles functionalized with hydrous lanthanum oxide. J. Colloid Interface Sci. 465, 76–82. doi:10.1016/j.jcis.2015.11.043.

Li, B., Shan, C.-L., Zhou, Q., Fang, Y., Wang, Y.-L., Xu, F., Han, L.-R., Ibrahim, M., Guo, L.-B., Xie, G.-L., Sun, G.-C., 2013. Synthesis, characterization, and antibacterial activity of cross-linked chitosan-glutaraldehyde. Mar. Drugs. 11, 1534–1552. doi:10.3390/md11051534.

Liu, J., Sun, Z., Deng, Y., Zou, Y., Li, C., Guo, X., Xiong, L., Gao, Y., Li, F., Zhao, D., 2009a. Highly water-dispersible biocompatible magnetite particles with low cytotoxicity stabilized by citrate groups. Angew. Chemie - Int. Ed. 48, 5875–5879. doi:10.1002/anie.200901566.

Liu, X., Hu, Q., Fang, Z., Zhang, X., Zhang, B., 2009b. Magnetic chitosan nanocomposites: A useful recyclable tool for heavy metal ion removal. Langmuir 25, 3–8. doi:10.1021/la802754t.

Long, F., Gong, J.L., Zeng, G.M., Chen, L., Wang, X.Y., Deng, J.H., Niu, Q.Y., Zhang, H.Y., Zhang, X.R., 2011. Removal of phosphate from aqueous solution by magnetic Fe-Zr binary oxide. Chem. Eng. J. 171, 448–455. doi:10.1016/j.cej.2011.03.102.

Lovern, S.B., Klaper, R., 2006. Daphnia magna mortality when exposed to titanium dioxide and fullerene (C60) nanoparticles. Environ. Toxicol. Chem. 25, 1132–1137. doi:10.1897/05-278r.1.

Lu, A.H., Salabas, E.L., Schüth, F., 2007. Magnetic nanoparticles: Synthesis, protection, functionalization, and application. Angew. Chemie - Int. Ed. 46, 1222–1244. doi:10.1002/anie.200602866.

Lyngsie, G., Penn, C.J., Hansen, H.C.B., Borggaard, O.K., 2014. Phosphate sorption by three potential filter materials as assessed byisothermal titration calorimetry. J. Environ. Manage. 143, 26–33. doi:10.1016/j.jenvman.2014.04.010.

Massart, R., 1981. Preparation of aqueous magnetic liquids in alkaline and acidic media. IEEE Trans. Magn. 17, 1247-1248. doi: 10.1109/TMAG.1981.1061188.

Mills, P., Snabre, P., 1994. Settling of a suspension of hard spheres. Europhys. Lett. 25, 651–656. doi:10.1209/0295-5075/25/9/003.

Monier, M., Ayad, D.M., Abdel-Latif, D.A., 2012. Adsorption of Cu(II), Cd(II) and Ni(II) ions by cross-linked magnetic chitosan-2-aminopyridine glyoxal Schiff's base. Colloids Surf., B. 94, 250–258. doi:10.1016/j.colsurfb.2012.01.051.

Monteiro, O.A.C., Airoldi, C., 1999. Some studies of crosslinking chitosan-glutaraldehyde interaction in a homogeneous system. Int. J. Biol. Macromol. 26,

119–128. doi:10.1016/S0141-8130(99)00068-9.

Murphy, J., Riley, J.P., 1962. A modified single solution method for the determination of phosphate in natural waters. Anal. Chim. Acta. 27, 31–36. doi:10.1016/S0003-2670(00)88444-5.

Neto, C.G.T., Giacometti, J.A., Job, A.E., Ferreira, F.C., Fonseca, J.L.C., Pereira, M.R., 2005. Thermal analysis of chitosan based networks. Carbohydr. Polym. 62, 97–103. doi:10.1016/j.carbpol.2005.02.022.

Nürnberg, G.K., 1996. Trophic state of clear and colored, soft- and hardwater lakes with special consideration of nutrients, anoxia, phytoplankton and fish. Lake Reserv. Manag. 12, 432–447. doi:10.1080/07438149609354283.

Oberdörster, E., 2004. Manufactured nanomaterials (fullerenes, C60) induce oxidative stress in the brain of juvenile largemouth bass. Environ. Health Perspect. 112, 1058–1062. doi:10.1289/ehp.7021.

Onyango, M.S., Kuchar, D., Kubota, M., Matsuda, H., 2007. Adsorptive removal of phosphate ions from aqueous solution using synthetic zeolite. Ind. Eng. Chem. Res. 46, 894–900. doi:10.1021/ie060742m.

Philippova, O., Barabanova, A., Molchanov, V., Khokhlov, A., 2011. Magnetic polymer beads: Recent trends and developments in synthetic design and applications. Eur. Polym. J. 47, 542–559. doi:10.1016/j.eurpolymj.2010.11.006.

Pillai, C.K.S., Paul, W., Sharma, C.P., 2009. Chitin and chitosan polymers: Chemistry, solubility and fiber formation. Prog. Polym. Sci. 34, 641–678. doi:10.1016/j.progpolymsci.2009.04.001.

Reddy, D.H.K., Lee, S.M., 2013. Application of magnetic chitosan composites for the removal of toxic metal and dyes from aqueous solutions. Adv. Colloid Interface Sci. 201-202, 68–93. doi:10.1016/j.cis.2013.10.002.

Reitzel, K., Hansen, J., Andersen, F., Hansen, K.S., Jensen, H.S., 2005. Lake restoration by dosing aluminum relative to mobile phosphorus in the sediment. Environ. Sci. Technol. 39, 4134–4140. doi:10.1021/es0485964.

Robb, M., Greenop, B., Goss, Z., Douglas, G., Adeney, J., 2003. Application of Phoslock^{TM}, an innovative phosphorus binding clay to two Western Australian waterways: Preliminary findings. Hydrobiologia 494, 237–243. doi:10.1023/A:1025478618611.

Rodrigues, S., da Costa, A.M.R., Grenha, A., 2012. Chitosan/carrageenan nanoparticles : Effect of cross-linking with tripolyphosphate and charge ratios tripolyphosphate and charge ratios. Carbohyd. Polym. 89, 282–289. doi:10.1016/j.carbpol.2012.03.010.

Sakadevan, K., Bavor, H.J., 1998. Phosphate adsorption characteristics of soils , slags and zeolite to be used as substrates in constructed wetland systems. Wat. Res. 32, 393–399.

Shaikh, A.M.H., Dixit, S.G., 1992. Removal of phosphate from waters by precipitation and high gradient magnetic separation. Water Res. 26, 845–852. doi:10.1016/0043-1354(92)90016-W.

Søndergaard, M., Jensen, J.P., Jeppesen, E., 2003. Role of sediment and internal loading of phosphorus in shallow lakes. Hydrobiologia 506-509, 135–145.

doi:10.1023/B:HYDR.0000008611.12704.dd.

Søndergaard, M., Kristensen, P., Jeppesen, E., 1992. Phosphorus release from resuspended sediment in the shallow and wind-exposed Lake Arreso, Denmark. Hydrobiologia 228, 91–99.

Sowmya, A., Meenakshi, S., 2014. Effective removal of nitrate and phosphate anions from aqueous solutions using functionalised chitosan beads. Desalin. Water Treat. 52, 2583–2593. doi:10.1080/19443994.2013.798842.

Sugimoto, T., Matijević, E., 1980. Formation of uniform spherical magnetite particles by crystallization from ferrous hydroxide gels. J. Colloid Interface Sci. 74, 227–243. doi:10.1016/0021-9797(80)90187-3.

Sun, Z., Su, F., Forsling, W., Samskog, P., 1998. Surface characteristics of magnetite in aqueous suspension. J. Colloid Interface Sci. 197, 151–9. doi:10.1006/jcis.1997.5239.

Tang, S.C.N., Lo, I.M.C., 2013. Magnetic nanoparticles: Essential factors for sustainable environmental applications. Water Res. 47, 2613–2632. doi:10.1016/j.watres.2013.02.039.

Tian, Y., Yu, B., Li, X., Li, K., 2011. Facile solvothermal synthesis of monodisperse Fe_3O_4 nanocrystals with precise size control of one nanometre as potential MRI contrast agents. J. Mater. Chem. 21, 2476. doi:10.1039/c0jm02913k.

Wong, Y.C., Szeto, Y.S., Cheung, W.H., McKay, G., 2004. Adsorption of acid dyes on chitosan - Equilibrium isotherm analyses. Process Biochem. 39, 693–702. doi:10.1016/S0032-9592(03)00152-3.

Wulff-Pérez, M., Torcello-Gómez, A., Gálvez-Ruíz, M.J., Martín-Rodríguez, A., 2009. Stability of emulsions for parenteral feeding: Preparation and characterization of o/w nanoemulsions with natural oils and Pluronic f68 as surfactant. Food Hydrocoll. 23, 1096–1102. doi:10.1016/j.foodhyd.2008.09.017.

Yao, W., Rao, P., Lo, I.M.C., Zhang, W., Zheng, W., 2014. Preparation of cross-linked magnetic chitosan with quaternary ammonium and its application for Cr(VI) and P(V) removal. J. Environ. Sci. (China) 26, 2379–2386. doi:10.1016/j.jes.2014.03.005.

Yavuz, C.T., Mayo, J.T., Yu, W.W., Prakash, A., Falkner, J.C., Yean, S., Cong, L., Shipley, H.J., Kan, A., Tomson, M., Natelson, D., Colvin, V.L., 2006. Low-field magnetic separation of monodisperse Fe_3O_4 nanocrystals. Science 314, 964–967.

Zamparas, M., Gianni, A., Stathi, P., Deligiannakis, Y., Zacharias, I., 2012. Removal of phosphate from natural waters using innovative modified bentonites. Appl. Clay Sci. 62-63, 101–106. doi:10.1016/j.clay.2012.04.020.

Zamparas, M., Zacharias, I., 2014. Restoration of eutrophic freshwater by managing internal nutrient loads. A review. Sci. Total Environ. 496, 551–562. doi:10.1016/j.scitotenv.2014.07.076.

Zhang, L.Y., Zhu, X.J., Sun, H.W., Chi, G.R., Xu, J.X., Sun, Y.L., 2010. Control synthesis of magnetic Fe_3O_4-chitosan nanoparticles under UV irradiation in aqueous system. Curr. Appl. Phys. 10, 828–833. doi:10.1016/j.cap.2009.10.002.

Zhang, W., Shen, F., Hong, R., 2011. Solvothermal synthesis of magnetic Fe_3O_4 microparticles via self-assembly of Fe_3O_4 nanoparticles. Particuology 9, 179–

186. doi:10.1016/j.partic.2010.07.025.

Zhou, Z.H., Xue, J.M., Wang, J., Chan, H.S.O., Yu, T., Shen, Z.X., 2002. $NiFe_2O_4$ nanoparticles formed in situ in silica matrix by mechanical activation. J. Appl. Phys. 91, 6015–6020. doi:10.1063/1.1462853.

Zhu, X., Wang, J., Zhang, X., Chang, Y., Chen, Y., 2010. Trophic transfer of TiO_2 nanoparticles from daphnia to zebrafish in a simplified freshwater food chain. Chemosphere, 79, 928-933.

Figures

Fig. 1. SEM micrographs of (a) MCMs and (b) cross-sectioned MCMs.

Fig. 2. Magnetic hysteresis curve of (a) Fe_3O_4 and (b) MCMs.

Fig. 3. Sedimentation ratio of carbonyl Fe microparticles (closed squares), and MCMs (open circles). H = sediment front determined at a constant value of transmission (5 %). H_0 = initial sample height (at time zero). Concentration: 0.72 g L^{-1} of carbonyl Fe particles/MCMs. pH = 7.

Fig. 4. Effect of pH on P removal efficiency (bars) and on electrophoretic mobility (square symbols) of MCMs. Initial concentrations: 0.72 g MCMs L^{-1} and 0.01 mM P. Standard deviation is represented by vertical error bars.

Fig. 5. Adsorption isotherm for Fe_3O_4 (open circles), MCMs (closed squares) and CMs (open triangles) at pH 7. Initial concentrations: 0.1 g Fe_3O_4 L^{-1}, 0.72 g MCMs L^{-1}, 0.62 g CMs L^{-1} and 0.01-0.16 mM P. Standard deviation is represented by vertical error bars.

Fig. 1

1a

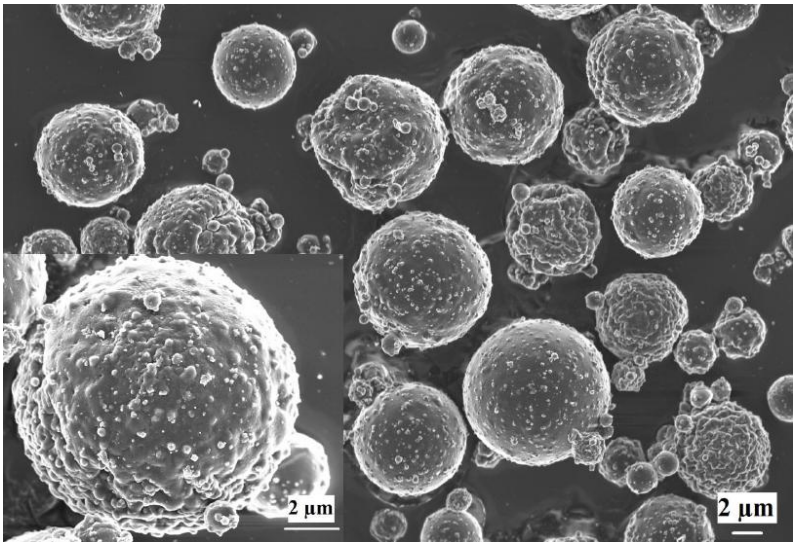

1b

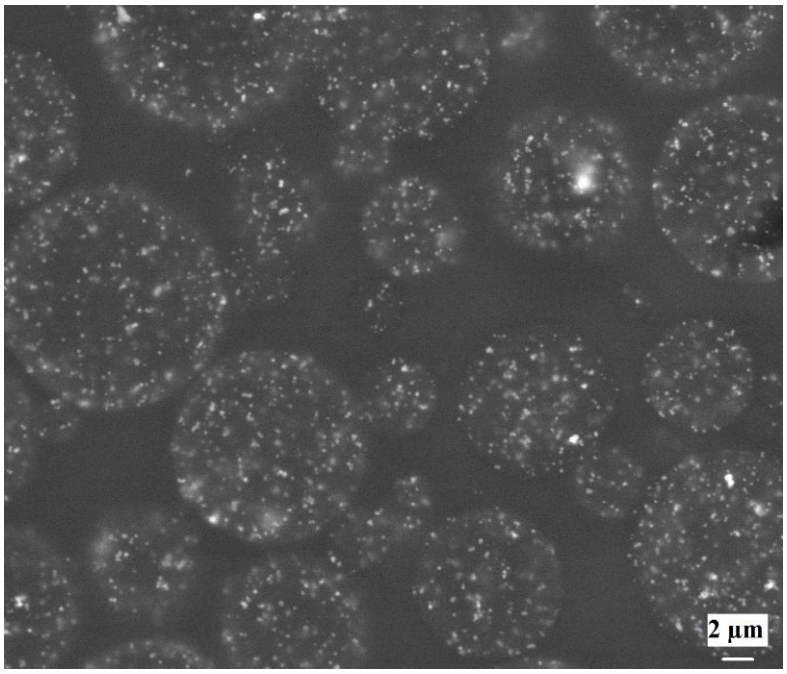

Fig. 2

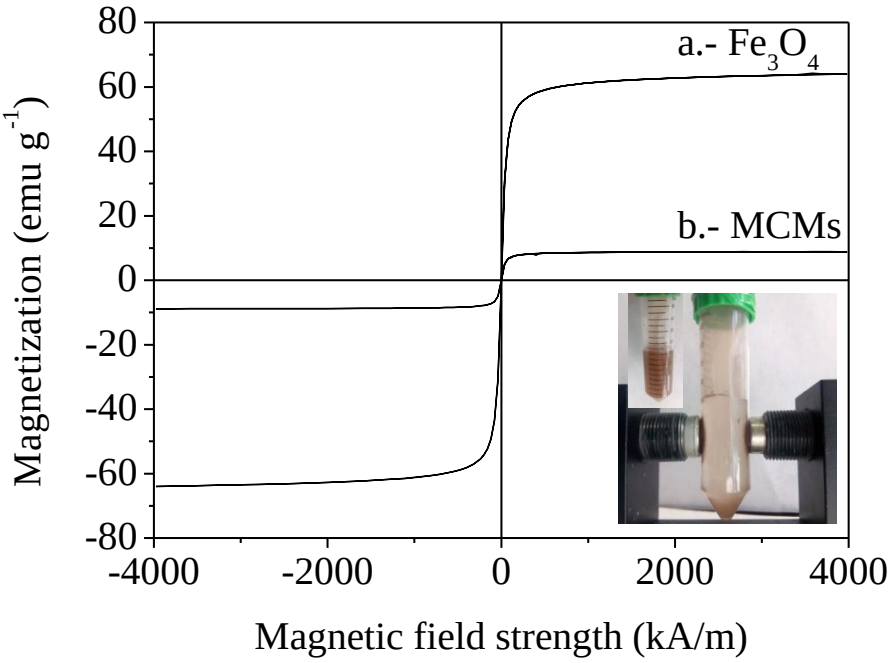
a.- Fe_3O_4
b.- MCMs
Magnetization (emu g^{-1})
Magnetic field strength (kA/m)
80
60
40
20
0
-20
-40
-60
-80
-4000
-2000
0
2000
4000

Fig. 3

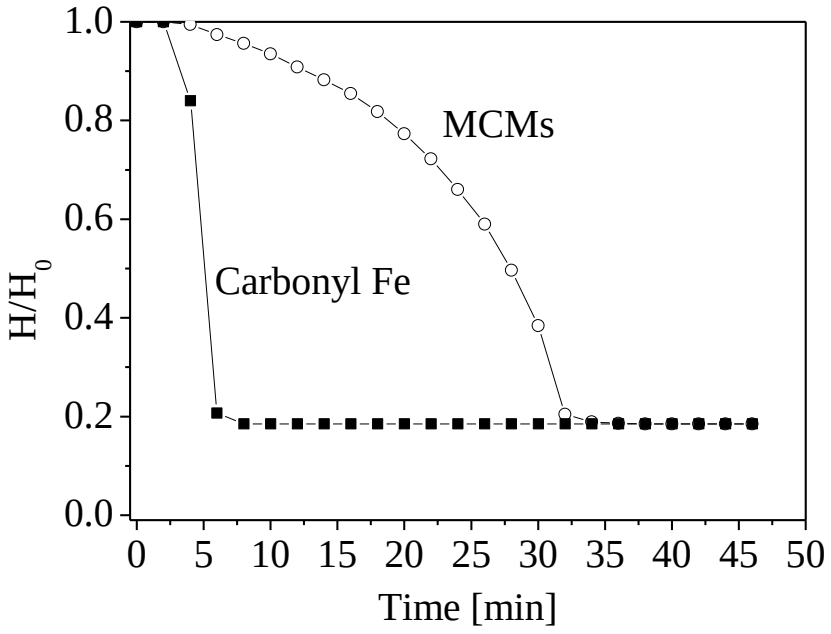
1.0
0.8
0.6
0.4
0.2
0.0
H/H0
MCMs
Carbonyl Fe
0
5
10
15
20
25
30
35
40
45
50
Time [min]

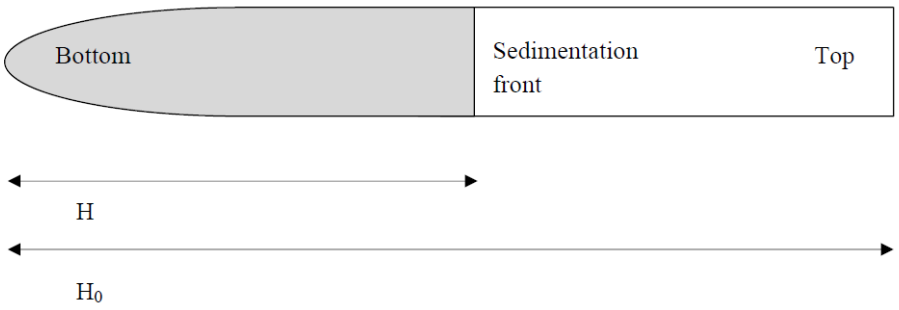
Bottom
Sedimentation front
Top
H
H0

Fig. 4

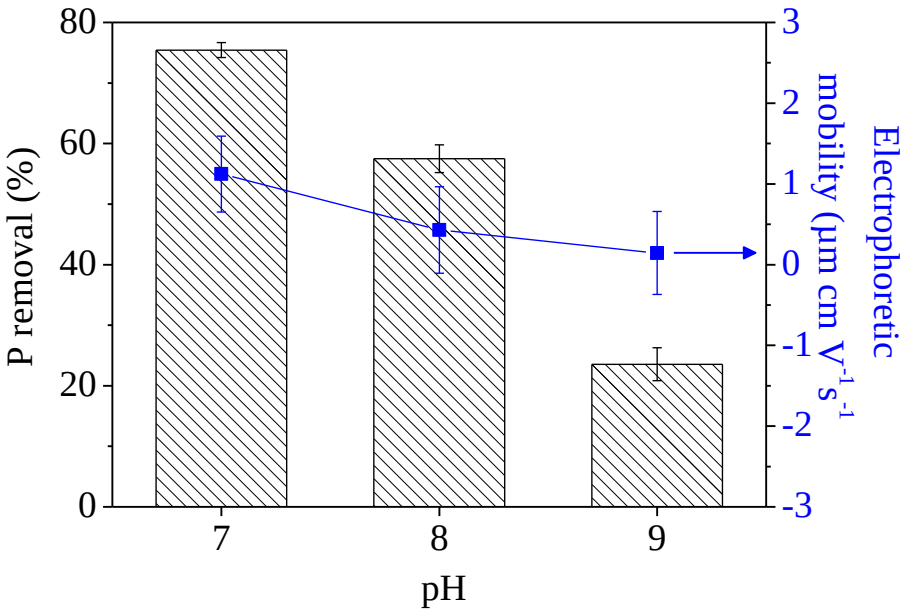
80
60
40
20
0
P removal (%)
3
2
1
0
-1
-2
-3
Electrophoretic mobility (μm cm V-1 s-1
7
8
9
pH

Fig. 5